Spin Polarization, Electron-Phonon Coupling and Zero-Phonon Line of the NV Center in 3C-SiC

Hans Jurgen von Bardeleben, Jean-Louis Cantin, Uwe Gerstmann, Wolf Gero G Schmidt, Timur Biktagirov

Spin Polarization, Electron-Phonon Coupling and Zero-Phonon Line of the NV Center in 3*C*-SiC

H. J. von Bardeleben,[1*] J. L. Cantin,[1] U. Gerstmann,[2] W. G. Schmidt,[2] T. Biktagirov[2**]

[1]*Sorbonne Université, Institut des Nanosciences de Paris, UMR 7588 au CNRS 4, place Jussieu, 75005 Paris, France*
[2]*Universität Paderborn, Department Physik, Warburger Str. 100, 33098 Paderborn, Germany*

[*] vonbarde@insp.jussieu.fr
[**] Timur.Biktagirov@upb.de

ABSTRACT: The nitrogen-vacancy (NV) center in 3*C*-SiC, the analog of the NV center in diamond, has recently emerged as a solid-state qubit with competitive properties and significant technological advantages. Combining first-principles calculations and magnetic resonance spectroscopy we provide thorough insight in its magneto-optical properties. By applying resonantly excited electron paramagnetic resonance spectroscopy, we identified the zero-phonon absorption line of the $^3A_2 \rightarrow {}^3E$ transition at 1289 nm (within the telecom O-band) and measured its phonon sideband, the analysis of which reveals a Huang-Rhys factor of S = 2.85 and a Debye-Waller factor of 5.8 %. The low temperature spin-lattice relaxation time was found to be exceptionally long (T_1 = 17 s at 4 K). All these properties make NV in 3*C*-SiC a strong competitor for qubit application. In addition, the strong variation of the zero-field splitting in the range of 4K to 380K allows its application for nanoscale thermal sensing.

KEYWORDS: *nitrogen-vacancy color centers, silicon carbide, resonant excitation, spin polarization, electron-phonon coupling*

The NV center in diamond has become the prototype of the solid-state qubits with multiple applications ranging from quantum computing to nanoscale sensing [1-3]. Theoretically predicted long time ago [4], NV centers in silicon carbide (SiC), i.e. nearest-neighbor silicon vacancy-nitrogen complexes, V_{Si}-N_C (Figure 1a), have recently been evidenced in different polytypes of SiC [5–10]. From a material point of view, SiC offers various advantages over diamond. The 4*H*-SiC is a semiconductor with a mature microelectronics technology, efficient *n*- and *p*-type doping possibilities [11], the disponibility of large-scale bulk substrates and epitaxial layers. Further, SiC nanostructures can easily be formed by etching techniques. The 3*C* polytype, less applied in microelectronics, has an additional interest as it can be epitaxied on silicon. This allows a potential direct connection between SiC and Si photonics and an integration of defect qubits in 3*C*-SiC into a wide variety of optical devices [12-14]. With high-fidelity spin-photon interfaces reported for spin qubits in this polytype [15], 3C-SiC represents a promising platform for quantum information and sensing applications.

The NV centers in SiC exhibit the same structural and electronic properties as its diamond counterpart. In the 1- charge state, they have a $^3A_2$ spin S = 1 ground state (configuration a^2e^2) with a zero-field splitting (ZFS) parameter D of (1.3±0.1) GHz (Figure 1b). Even though the NV centers in SiC have the same microstructure as the one's in diamond, they differ from them by their intrinsic magneto-optical signatures and the semiconducting properties of the SiC material [16, 17]. Some common aspects are a spin-triplet ground state, a narrow zero-phonon emission line corresponding to a radiative recombination from the first excited state ^3E (configuration a^1e^3) to the $^3A_2$ ground state, the presence of an intermediated singlet state, giving rise to optically induced ground-state spin polarization, and long spin coherence times. These properties will allow their application as solid-state qubits [18,19].

Most applications of NV centers are based on optical spectroscopy of the zero-phonon line (ZPL), and the analysis of the spin states, when the system is submitted to various

perturbations [20–21]. In the case of NV centers in diamond the ZPL is in the visible spectral range with a ZPL emission line at 637 nm, whereas in the SiC polytypes they are shifted to the near infrared range (NIR) between 1100 nm and 1300 nm, which are more suitable for device applications due to the low loss of transmission in optical waveguides.

The closest analog to the NV center in diamond is the NV center in 3*C*-SiC, which has equally a cubic, i.e. zinc blende, crystal structure. NV centers in diamond and 3*C*-SiC give thus rise to one unique defect configuration with C_{3v} symmetry and four possible equivalent [111] oriented configurations. In the hexagonal polytypes (4*H*, 6*H*) of SiC more than one NV centers exist, four in 4*H* and six in 6*H*, depending of the lattice sites of the vacancy and the nitrogen atoms. They are characterized by slightly different magneto-optical and symmetry properties and all of them show a narrow zero-phonon emission line, as required for solid-state qubit application.

The association of a ZPL with a particular paramagnetic center is not trivial as often more than one ZPL are present in these samples. We have shown recently in the case of NV centers in 4*H*- and 6*H*-SiC, that the combination of resonant optical excitation and EPR spectroscopy allows the direct assignment of a particular ZPL line to the associated NV center [22, 23]. The use of tunable lasers with high spectral resolution below nm and an output power of up to 30 mW has been shown to be particularly suited for such studies as the ZPL were found to be narrow with sub_nanometer structure. High laser powers can be necessary as the goundstate spin polarization depends on the competition between optical feeding and thermal relaxation.

In 3*C*-SiC resonant excitation spectroscopy of the NV center has not yet been reported and the ZPL has been only indirectly attributed [9] based on available theoretical predictions. In that photoluminescence study, two ZPL emission lines at 1289 nm and 1468 nm were simultaneously observed in samples where the NV center had been generated by high energy particle irradiation. In that work the ZPL at 1468nm had been tentatively associated with the NV center [9]. To further investigate this assignment we have performed now resonant optical excitation EPR spectroscopy with a high resolution tunable IR laser. Our results show that only the 1289 nm ZPL is related with the $^3A_2 \rightarrow {}^3E$ transition of the NV center, and allows us to assign it to the NV center. In addition they allowed us to monitor the associated phonon sideband from which we deduce a Debye-Waller factor of >5 %. In time resolved EPR measurements we determined the low-temperature spin-lattice relaxation time T_1 of the NV center and found values >10ms at T=4K. These properties make the NV center in 3C-SiC a favorable defect for quantum technological applications.

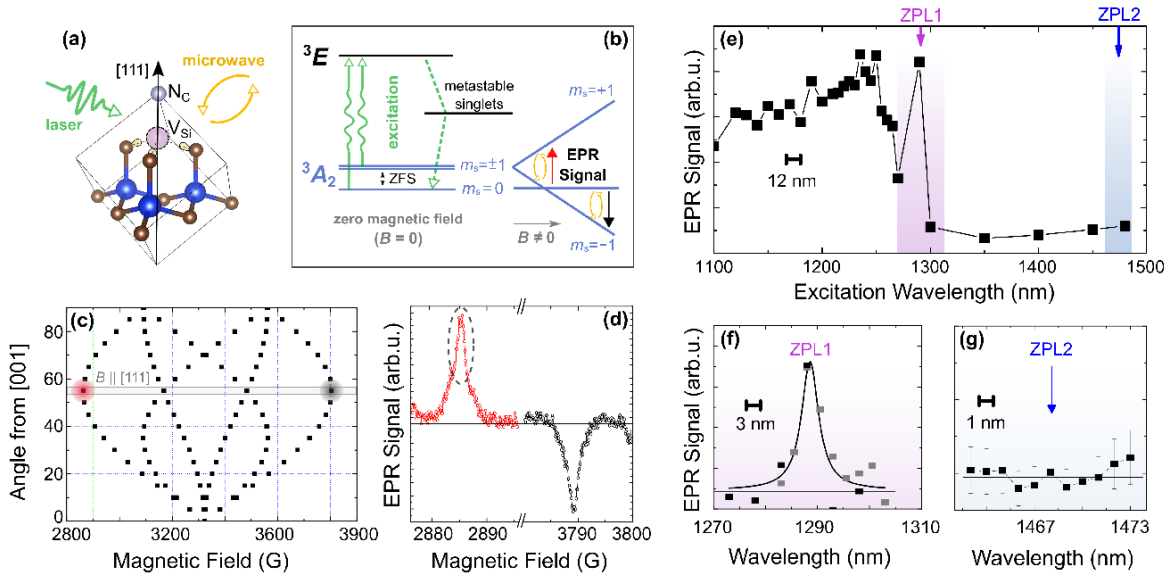

Fig. 1. Resonant optical excitation experiment. (a) Schematic atomic structure of the NV center aligned with the crystallographic [111] direction of 3*C*-SiC. (b) energy level diagram illustrating the ground and excited states and the optically induced groundstate spin polarization. Applied magnetic field causes Zeeman splitting of $^3A_2$; the preferential population of the $|m_S = 0\rangle$ level will invert the phases (absorption/emission) of the low- and high-field EPR transitions $|m_S = 0\rangle \rightarrow |m_S \pm 1\rangle$. (c) Angular variation of the NV center resonance fields for a rotation of the applied magnetic field in the (110) plane. The resonance fields of the [111] aligned NV center are highlighted. (d) Low-temperature (*T* = 4 K) EPR spectrum of the [111] aligned NV center under resonant optical excitation. The optically induced ground state spin polarization results in an absorption and emission lineshape for the low-field and high-field lines respectively with a close to100 % spin polarization. The low-field EPR line at 2870 G is used for the resonant excitation measurements. (e) Large-scale excitation spectrum of the EPR signal intensity measured with a resolution of 12 nm; (f) high-resolution excitation spectra of the NV center at the ZPL1 at 1289 nm (ZPL1) and (g) and the ZPL2 at 1468 nm. Only the ZPL1 is related with the NV center.

Resonant optical excitation spectroscopy. The angular variation of the EPR transitions of the NV centers for a rotation of the magnetic field, **B**, in the (110) plane of 3*C*-SiC is shown in Figure 1c. We analyze the observed transitions with the standard spin Hamiltonian:

$$H = D(S_z^2 - S(S+1)/3) + \mu_B \mathbf{B} \cdot \mathbf{g} \cdot \mathbf{S} + \mathbf{S} \cdot \boldsymbol{A} \cdot \boldsymbol{I}, \qquad (1)$$

where z is the threefold symmetry axis of the NV center, *D* the ZFS parameter, **S** the electron spin operator (with the eigenvalue *S* = 1), **g** the *g*-tensor that includes higher order contributions to the free electron *g*-factor, μ_B is the Bohr magneton and **A** the hyperfine interaction HF tensor. The corresponding spin Hamiltonian parameters of the NV center have been reported before [7–9] and are compared in Table 1 with those of the NV center in diamond. For **B** parallel to the [111] direction, the EPR spectrum simplifies to two doublets, corresponding to one NV center whose symmetry axis is aligned with the applied magnetic field and the three equivalent NV centers, whose axes are at 109° (see also Figure S1). The EPR spectra show a multiplet structure due to hyperfine (HF) interaction with the spin I = 1 ^{14}N nearest neighbor atom, a fingerprint of all NV centers in SiC and in diamond (see Figure S2).

Table 1. Comparison of the main spin Hamiltonian parameters of the NV centers in 3*C*-SiC and diamond: ground state configuration, point symmetry, g-tensor, ^{13}C HF interaction, ^{14}N HF interaction, zero field splitting parameter and zero phonon line wavelength; first line experiment, second line DFT calculated values, third line parameters for the NV center in diamond

	ground state	symmetry	*g*-tensor	^{13}C HF (MHz)	^{14}N HF (MHz)	ZFS, *D* (MHz)	ZPL (nm)
3*C*-SiC	$^3A_2$	C_{3v}	$g_{\|\|}$=2.0030 $g_\perp$=2.0028		± 1.2	1306 (T=4K)	1289
DFT	$^3A_2$	C_{3v}	$g_{\|\|}$=2.0034 $g_\perp$=2.0029	70.28	– 1.08	1295.8	1285
Diamond	$^3A_2$	C_{3v}	$g_{\|\|}$=2.0030 $g_\perp$=2.0028	130	± 2.3	2800	637

The optical excitation experiments were performed in the configuration **B**||[111]; the analysis is based on the optically induced variation of the EPR signal intensity of the [111] oriented NV center (Figure 1d). All resonant excitation measurements were done at T = 4 K. For each monochromatic excitation we measured the intensity of the NV center line. In Figure 1e, we show the result of a wide scan from 1500 nm to 1100 nm and in Figures 1f and 1g the results of high-resolution scans around the positions of the previously measured photoluminescence ZPL1, ZPL2 lines. The result presented in Figure 1e-g do not show any response of the NV center for wavelengths longer than 1300 nm excluding the association with the ZPL2 line, but show a strong response at the wavelength of ZPL1 and further reveal its phonon sideband. As expected, the resonantly excited EPR spectroscopy allow to link directly the ZPL line with the paramagnetic NV center. As the ZPL lines in SiC have been found to be narrow (≈1 nm), we have further verified the absence of any response at ZPL2 with a high resolution (0.5 nm) tunable IR laser (see also Figure 1g). Despite the high resolution and a high available excitation power of 20 mW we did not observe any response of the NV center in this range. Thus, we can conclude that ZPL2 is not linked with the paramagnetic $^3A_2 \rightarrow {}^3E$ transition of the NV center.

Focusing on the ZPL1, we measured the excitation spectrum with increased resolution of 6 nm and 3 nm. As shown in Figure 1f, the resonant excitation spectrum is centered at the ZPL at 1289 nm with a width of 5 nm. The resolution of the monochromator did not allow to further decrease this value and its width is limited by the resolution of the excitation system. Analyzing the low- and high-field EPR lines of the NV center (see Figure 1d) we deduce an optically induced ground state spin polarization P of nearly 100% at T=4K for an excitation at 1289nm. P is defined as $P = I_{low} - I_{high}/(I_{low} + I_{high})$, where I_{low} and I_{high} are the intensities of the low and high field resonance line respectively. From this experimental result we attribute the ZPL1 at 1289 nm to the NV center and based on our calculations to the $^3A_2 \rightarrow {}^3E$ intracenter transition. In Figure 2 we show an overwiew of the NV center ZPL lines in diamond and the SiC polytypes. The broad multiplet structure spectrum at lower wavelength is attributed to the phonon assisted transitions of ZPL1 as confirmed by our calculations. Notably, the ZPL of NV in 3*C*-SiC thus falls into the technologically relevant O-band. This makes it compatible with another recently emerged promising class of spin qubits in SiC, which also emits in the O-band, i.e., the vanadium center [24, 25].

It is remarkable, that a nearly 100 % spin polarization of the NV ground state is obtained even though the excitation power in the high-resolution measurement at 1289 nm is very low (< 1μW). As the spin polarization observed in the CW EPR experiment is a competition between optical feeding in the $|m_S = 0\rangle$ groundstate and thermal relaxation (T_1), this is an indication of long spin lattice relaxation times T_1, which we have studied in the following in more detail.

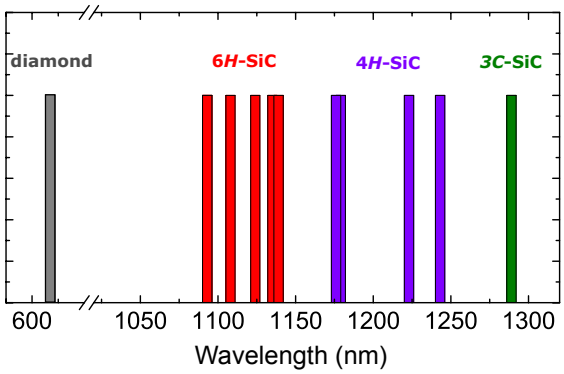

Fig. 2. Overview of the NV center ZPL in diamond and in three polytypes of SiC. In diamond, the ZPL is located in the visible spectral range, whereas in SiC they are shifted to the telecom wavelength compatible with low-loss optical waveguides (4*H*-SiC data from Ref. 22, 6*H*-data from Ref. 23, and 3*C*-SiC this work).

Electron-phonon interactions. The phonon-assisted absorption band contains interesting information on the phonon coupling of the $^3A_2 \rightarrow {}^3E$ optical transitions. Recent ODMR studies [26–29] of the structurally related, $S = 1$ neutral divacancy centers in 4*H* and 6*H*-SiC had shown, that the phonon sideband of their ZPL lines could be simulated by a superposition of 35 meV separated phonon replica. Although the common assumption of one local phonon mode contributing to the phonon sideband provides a reasonable approximation (see also Refs. [26, 27] for discussion), here we have analyzed the phonon sideband of the excitation spectrum of the NV center considering all vibrational modes of the defect and bulk phonons [30].

First, we have calculated the *partial* Huang-Rhys factors, S_k (Eq. 2), along with the spectral density of electron-phonon coupling, $S(\hbar\omega)$ (Eq. 3), shown in Figure 3a. The value of S_k describes the interaction strength of an electronic defect state with the vibrational modes of the surrounding lattice and can be interpreted as the average number of phonons with frequency ω_k emitted during an electronic transition. As can be seen from the plot in Figure 3a, there are *two* dominant vibrational contributions to the $^3A_2 \rightarrow {}^3E$ transition of the NV center in 3*C*-SiC. The most pronounced peak in $S(\hbar\omega)$ is due to the collective contribution of the acoustic and optical bulk modes with energies below 50 meV. The phonon modes constituting this peak are relatively delocalized (inverse participation ratio > 150). Next, the localized defect-related vibrational modes (inverse participation ratio < 100) contribute to a smaller peak around 70 meV. There is also a distinct band of localized vibrational modes at the high-frequency edge around 110 meV. However, these modes are only weakly coupled to the $^3A_2 \rightarrow {}^3E$ transition displacement.

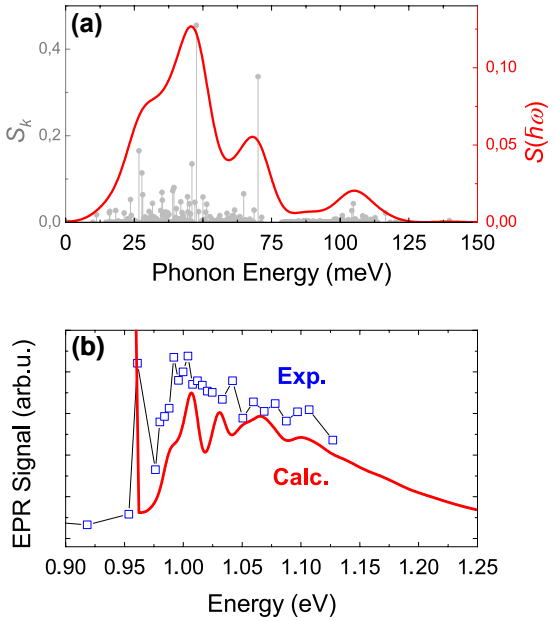

Fig. 3. Electron-phonon interactions of the NV center. (A) Calculated partial Huang-Rhys factors S_k (gray) and the spectral density $S(\hbar\omega)$ of electron-phonon coupling (red). (B) Experimental high-resolution excitation spectrum of the NV center in 3*C*-SiC (blue) compared with the calculated spectral function (red).

In Figure 3b, we compare the spectral function calculated based on the entire electron-phonon spectral density (see the Methods section for detail) with the experimental excitation spectrum; the spectra are plotted on an energy scale. We observe a good agreement with the first phonon assisted transition separated from the ZPL by about 40 meV. The structure of the broad phonon sideband mimics a superposition of multiple phonon-assisted transitions separated by 35-40 meV, in accordance with the peak in $S(\hbar\omega)$. Very similar results for the phonon coupling were reported for the silicon vacancy and divacancy centers in 4*H*-SiC [26–29]. We have equally reanalyzed the excitation spectrum of the quasicubic NV center in 4*H*-SiC, see Figure S3) and found a similar phonon coupling. Apparently, Si monovacancies, divacancies and NV centers in SiC all share the same properties of (i) a sharp ZPL separated from the phonon sideband by 35-40 meV, (ii) a broad phonon sideband with a width ranging from 200 to 500 meV, (iii) a partially resolved structure of the phonon sideband.

From our calculations we deduce a *total* Huang-Rhys factor of S = 2.85 indicating the average number of phonons emitted during the electronic transition. This value allows us to predict the weight of the ZPL relative to the total spectral intensity, i.e. the Debye-Waller factor, as $w_{ZPL} = e^{-S}$ [30]. The obtained Debye-Waller factor is 5.8%, which is larger than the 3.2% measured for the diamond NV center [30] and thus favorable for applications as solid-state qubit.

Time-resolved spin dynamics. As the high spin polarization of the NV center groundstate indicated a long spin lattice relaxation time T_1, we have attempted to measure its value directly by EPR spectroscopy. Our setup allows a time resolution of 100 ms. The experimental results at T = 4 K are shown in Figure 4a-b, and in Figure S4 for the measurements at 10 K. The decline of the ground-state spin polarization after resonant excitation at 1289 nm can be described by a simple exponential decline with a time constant of 17 s, which corresponds to the spin-lattice relaxation time constant T_1 (see Figure 4b). Its value is comparable to the case of the NV centers in diamond [31–33].

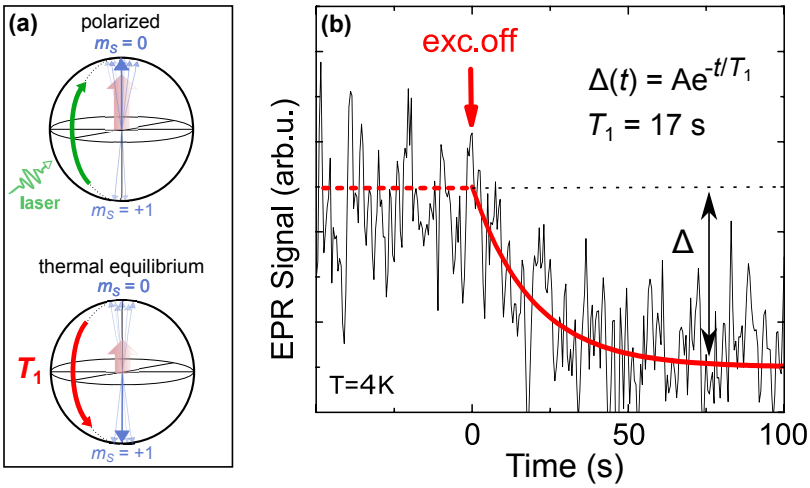

Fig. 4. Decline of the ground state spin polarization. (A) Simplified sketch of the distribution of Bloch vectors with (top) and without (bottom) resonant optical excitation illustrating the population difference between the $|m_S = 0\rangle$ and $|m_S \pm 1\rangle$ ground-state spin sublevels. Without excitation, spin-lattice relaxation drives the populations towards thermodynamic equilibrium with the time constant T_1. (B) Time-resolved EPR signal intensity at T = 4 K after switch-off of the optical excitation. Red line shows the fit with a single exponential decline with the time constant T_1=17s.

The *spin lattice relaxation time* is an important property of NV centers as it will limit or allow applications such as dynamic decoupling or sensing [34]. In general, it is associated with the electron-phonon interaction and describes the energy dissipation to the crystal lattice [35]. At low temperature, its value is only partially electron-phonon-coupling induced, while substantial contribution from spin-spin interactions with neighboring nuclear or electron spins becomes dominant [36]. Our sample had a natural isotopic abundance of Si and C; the use of isotopically purified samples can be expected to increase this value still further. Also electron spin interactions in samples with high defect concentrations can reduce the T_1 parameter; in our samples the concentration of the NV centers is estimated to 10^{15} to 10^{16} cm^{-3}. Lower defect concentrations, requiring application of the more sensitive ODMR spectroscopy, can also improve this value further. As the measurements were done at a magnetic field of 2870 G, the ground state level anticrossing (GLAC) effects occuring in the magnetic field range B < 1000 G are not operative. For the actively studied axial divacancy centers in 4*H*-SiC, Lindvall et al. [34] recently predicted the T_1 values of the order of 0.5 s, which is about an order of magnitude smaller than the value obtained for the NV center in 3*C*-SiC.

Temperature dependence of the ZFS. In the case of the NV center in diamond the temperature dependence of the ZFS parameter D has been shown to be a useful tool for local temperature measurements [37–40]. We have thus also investigated the variation $D(T)$ for the NV center in 3*C*-SiC and compared it with the case of the diamond NV. As shown in Figure 5a, we observe a monotonous and non-linear decrease of D, which can be fitted with a polynomial function $D(T) = D_0 + D_1T + D_2T^2 + D_3T^3$. From the fit we obtain the coefficients D_0 = 1306 MHz, $D_1 = -2.7 \cdot 10^{-3}$ MHz/K, $D_2 = -2.3 \cdot 10^{-4}$ MHz/K^2, and $D_3 = 1.8 \cdot 10^{-7}$ MHz/K^3. The temperature variation of D for the NV center in 3*C*-SiC is substantially higher compared to its diamond counterpart. In the studied temperature range between 4 K and 360 K, the total change of D is 25 MHz, while it is only 7 MHz for the diamond case.

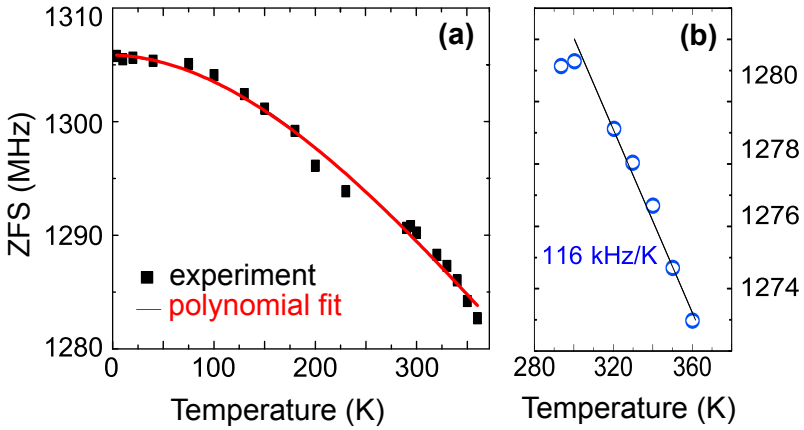

Fig. 5. Temperature dependence of the ZFS parameter *D*. (A) Large-scale temperature variation fit with a polynomial function of order 3 (red line). (B) Temperature variation of the ZFS for $T > 300$ K.

As discussed by Doherty et al. [39], the variation of the ZFS parameter *D* has two contributions, thermal expansion of the lattice constants and the electron-phonon coupling. For the NV center in diamond, the thermal expansion can account only for about 15% of the observed thermal shift of *D* [40]. Here, we used the experimental thermal expansion coefficients reported in Ref. [41] and modeled this contribution for the NV center in 3*C*-SiC. In contrast to the NV center in diamond, we find that the thermal expansion contribution is more significant in the case of 3*C*-SiC (see Fig. S5). In the considered temperature range between 4 K and 360 K, this contribution alone gives rise to the total change in the *D* value of 12 MHz, which is already more than the entire thermal shift reported for the diamond counterpart.

Most practical applications are focused on the high-temperature range above $T > 300$ K, where $D(T)$ of the diamond NV center is quasilinear. For this reason, we show in more detail the temperature variation of *D* for $T > 300$ K also for the case of 3*C*-SiC (Figure 5b). In analogy with the NV in diamond, we apply a simple linear approximation and find the slope dD/dT of 116 kHz/K. This is superior to the case of diamond NV, where the slope is 86 kHz/K. This value, superior to the case of NV in diamond, makes it promising for the use nanoscale thermometry with increased resolution.

Conclusion. The NV center in 3*C*-SiC has been shown to have remarkable magneto-optical properties, which make it an interesting alternative to the outstanding NV center in diamond, which is considered as a reference in quantum technology applications. A ZPL in the NIR range (within the telecom O-band) with a Debye-Waller factor of > 5 % and spin lattice relaxation times > 10 s are highly competitive parameters. Strong temperature variation of its ZFS offers paves the way to the use of this defect for nanoscale thermometry. Its good compatibility with Si technology due to easy heteroepitaxial growth is a further major advantage. More generally the NV centers in the cubic and previously studied hexagonal (4*H*, 6*H*) polytypes of SiC represent a set of centers with multiple applications in photonics and quantum technology.

SUPPORTING INFORMATION

Methods; X-band room temperature EPR spectrum without optical excitation; comparison of the hyperfine interaction parameters of the NV centers in 3*C*-SiC and diamond; High resolution excitation spectrum of the NV center in 4*H*-SiC, decline of the ground state spin

polarization at T = 10 K, Comparison of the experimental temperature variation of D with the DFT modeling involving only the thermal expansion.

ACKNOWLEDGMENTS

Numerical calculations were performed using grants of computer time from the Paderborn Center for Parallel Computing (PC^2) and the HLRS Stuttgart. The Deutsche Forschungsgemeinschaft (DFG) is acknowledged for financial support via the priority program SPP 1601 and the Transregional Collaborative Research Center TRR 142 (Project No. 231447078).

REFERENCES

1. Doherty, M. W.; Masson, N. B.; Delaney, P.; Jelezko, F.; Wrachtrup, J.; Hollenberg, L. C. L. The Nitrogen Vacancy Colour Center in Diamond. *Phys. Reports* **2013**, *528*, 1.
2. Weber, J. R.; Koehl, W. F.; Varley, J. B.; Janotti, A.; Buckley, B. B.; Van de Walle, C. G.; Awschalom, D. D. Quantum computing with defects. *PNAS* **2010**, 107, 8513-8518.
3. Rembold, P.; Oshnik, N.; Müller, M. M.; Montangero, S.; Calarco, T.; Neu, E. Introduction to Quantum Optimal Control for Quantum Sensing with Nitrogen Vacancy Centers in Diamond. *AVS Quantum Sci*. **2020**, *2*, 024701.
4. Gerstmann, U.; Rauls, E.; Frauenheim, Th.; Overhof, H. Formation and Annealing of Nitrogen-related Complexes in SiC. *Phys. Rev. B* **2003**, 67, 205202.
5. von Bardeleben, H. J.; Cantin, J. L.; Rauls, E.; Gerstmann, U. Identification and Magneto-optical Properties of the NV Center in 4*H*-SiC. *Phys. Rev. B* **2015**, *92*, 064104.
6. Zargaleh, S. A.; Eble, B.; Hameau, S.; Cantin, J.-L.; Legrand, L.; Bernard, M.; Margaillan, F.; Lauret, J.-S.; Roch, J.-F.; von Bardeleben, H. J.; *et al*. Evidence for Near-infrared Photoluminescence of Nitrogen Vacancy Centers in 4*H*-SiC. *Phys. Rev. B* **2016**, *94*, 060102(R).
7. von Bardeleben, H. J.; Cantin, J. L.; Csóré, A.; Gali, A.; Rauls, E.; Gerstmann, U. NV Centers in 3*C*, 4*H*, and 6*H* Silicon Carbide: A Novel Platform for Solid-state Qubits and Nanosensors. *Phys. Rev. B* **2016**, 94, 121202(R).
8. Csóré, A.; von Bardeleben, H. J.; Cantin, J. L.; Gali, A. Characterization and Formation of NV Centers in 3*C*, 4*H*, and 6*H*-SiC: An Ab-initio Study. *Phys. Rev. B* **2017**, *96*, 085204.
9. Zargaleh, S. A.; Hameau, S.; Eble, B.; Margaillan, F.; von Bardeleben, H. J.; Cantin, J. L.; Gao, W. Nitrogen Vacancy Center in Cubic Silicon Carbide: A Promising Qubit in the 1.5 μm Spectral Range for Photonic Quantum Networks. *Phys. Rev. B* **2018**, *98*, 165203.
10. Mu, Z.; Zargaleh, S. A.; von Bardeleben, H. J.; Fröch, J. E.; Nonahal, M.; H. Cai, Yang, X.; Yang, J.; Li, X.; Aharonovich, I.; Gao, W. Coherent Manipulation with Resonant Excitation and Single Emitter Creation of Nitrogen Vacancy Centers in 4*H* Silicon Carbide. *Nano Lett.* **2020**, *20*, 6142-6147.
11. Anderson, C. P.; Bourassa, A.; Miao, K. C.; Wolfowicz, G.; Mintun, P. J.; Crook, A. L.; Abe, H.; Hassan, J. U.; Son, N. T.; Ohshima, T.; Awschalom, D. D. Electrical and optical control of single spins integrated in scalable semiconductor devices. *Science* **2019**, 366, 1225-1230.
12. Zorman, C. A.; Fleischman, A. J.; Dewa, A. S.; Mehregany, M.; Jacob, C.; Nishino, S.; Pirouz, P. Epitaxial Growth of 3C-SiC Films on 4 in. Diam (100) Silicon Wafers by Atmospheric Pressure Chemical Vapor Deposition. *J. Appl. Phys*. **1995**, 78, 5136.
13. Radulaski, M.; Babinec, T. M.; Buckley, S.; Rundquist, A.; Provine, J.; Alasaad, K.; Ferro, G.; Vučković, J. Photonic Crystal Cavities in Cubic (3*C*) Polytype Silicon Carbide Films. *Opt.* Express **2013**, *21*, 32623-32629.
14. Calusine, G.; Politi, A.; Awschalom, D. D. Silicon Carbide Photonic Crystal Cavities with Integrated Color Centers. *Appl. Phys. Lett*. **2014**, 105, 011123.
15. Christle, D. J.; Klimov, P. V.; Charles, F.; Szász, K.; Ivády, V.; Jokubavicius, V.; Hassan, J. U.; Syväjärvi, M.; Koehl, W. F.; Ohshima, T.; Son, N. T. Isolated spin qubits in SiC with a high-fidelity infrared spin-to-photon interface, *Phys. Rev. X* **2017**, 7, 021046.

16. Awschalom, D. D.; Hanson, R.; Wrachtrup, J.; Zhou, B. B. Quantum Technologies with Optically Interfaced Solid-state Spins. *Nat. Photonics* **2018**, *12*, 516.
17. Atatüre, M.; Englund, D.; Vamivakas, N.; Lee, S. Y.; Wrachtrup, J. Material Platforms for Spin Based Photonic Quantum Technologies. *Nat. Rev. Mater.* **2018**, *3*, 38.
18. Wolfowicz, G.; Heremans, F. J.; Anderson, C. P.; Kanai, S.; Seo, H.; Gali, A.; Galli, G.; Awschalom, D. D. Quantum guidelines for solid-state spin defects. *Nat. Rev. Mater.* **2021**, 1-20.
19. Lohrmann, A.; Johnson, B. C.; McCallum, J. C.; Castelletto, S. A Review on Single Photon Sources in Silicon Carbide. *Rep. Prog. Phys.* **2017**, *80*, 034502.
20. Kraus, H.; Soltamov, V. A.; Fuchs, F.; Simin, D.; Sperlich, A.; Baranov, P. G.; Astakhov, G. V.; Dyakonov, V. Magnetic Field and Temperature Sensing with Atomic-scale Spin Defects in Silicon Carbide. *Sci. Rep.* **2014**, *4*, 5303.
21. Zhou, Yu; Wang, J.; Zhang, X.; Li, Ke; Cai, J.; Gao, W. Self-protected Thermometry with Infrared Photons and Defect Spins in SiC. *Phys. Rev. Applied* **2017**, *8*, 044015.
22. Zargaleh, S. A.; von Bardeleben, H. J.; Cantin, J. L.; Gerstmann, U.; Hameau, S.; Eble, B.; Gao, W. Electron Paramagnetic Resonance Tagged High-resolution Excitation Spectroscopy of NV^- Centers in 4*H*-SiC. *Phys. Rev. B* **2018**, *98*, 214113.
23. Khazen, Kh.; von Bardeleben, H. J.; Zargaleh, S. A.; Cantin, J. L.; Zhao, Mu; Gao, W.; Biktagirov, T.; Gerstmann, U. High-resolution Resonant Excitation of NV Centers in 6*H*-SiC: A Matrix for Quantum Technology Application. *Phys. Rev. B* **2019**, *100*, 205202.
24. Wolfowicz, G.; Anderson, C. P.; Diler, B.; Poluektov, O. G.; Heremans, F. J.; Awschalom, D. D. Vanadium spin qubits as telecom quantum emitters in silicon carbide. *Sci. Advances* **2020**, 6, eaaz1192.
25. von Bardeleben, H. J.; Zargaleh, S. A.; Cantin, J. L.; Gao, W. B.; Biktagirov, T.; Gerstmann, U. Transition metal qubits in 4 H-silicon carbide: A correlated EPR and DFT study of the spin *S*=1 vanadium V^{3+} center. *Phys. Rev. Mater.* **2019**, 3, 124605.
26. Shang, Z.; Berecen, Y.; Hollenbach, M.; Zhou, S.; Kraus, H.; Oshima, T.; Astakhov, G. V. Microwave Assisted Spectroscopy of Vacancy Related Spin Centers in Hexagonal SiC. *Phys. Rev. Applied* **2021**, *15*, 034059.
27. Shang, Z.; Hashemi, A.; Berencen, Y.; Komsa, H. P.; Erhart, P.; Zhou, S.; Helm, M.; Krasheninnikov, A. V.; Astakhov, G. V. Local Vibrational Modes of the Si Vacancy Spin Qubits in SiC. *Phys. Rev. B* **101**, *144109* (2020)
28. Banks, H. B.; Soykal, O. O.; Myers-Ward, R. L.; Gaskill, D. K.; Reineke, T. L.; Cartner, S. G. Resonant Optical Spin Initialization and Readout of Single Silicon Vacancies in 4*H*-SiC. *Phys. Rev. Applied* **2019**, *11*, 024013.
29. Hashemi, A.; Linderälv, C.; Kracheninnikov, A. V.; Ala-Nissila, T.; Erhart, P.; Komsa, H. P. Photoluminescnce Lineshapes for Color Centers in Silicon Carbide from Density Functional Theory Calculations. *Phys. Rev. B* **2021**, *103*, 125203.
30. Alkauskas, A.; Buckley, B. B.; Awschalom, D. D.; Van de Walle, C. G. First-principles Theory of the Luminescence Lineshape for the Triplet Transition in Diamond NV Centres. *New J. Phys.* **2014**, *16*, 073026.
31. Jarmola, A.; Acosta, V. M.; Jensen, K.; Chemerisov, S.; Budker, D. Temperature- and Magnetic-Field-Dependent Longitudinal Spin Relaxation in Nitrogen-Vacancy Ensembles in Diamond. *Phys. Rev. Lett.* **2012**, *108*, 197601.
32. de Guillebon, T.; Vindolet, B.; Roch, J. F.; Jacques, V.; Rondin, L. Temperature Dependence of T_1 Spin Relaxation of Single NV Centers in Nanodiamond. *Phys. Rev. B* **2020**, *102*, 165427.
33. Gugler, J.; Astner, T.; Angerer, A.; Schmiedmayer, J.; Majer, J.; Mohn, P. *Ab-initio* Calculation of Spin Lattice Relaxation Time T_1 for Nitrogen Vacancy Centers in Diamond. *Phys. Rev. B* **2018**, *98*, 214442.
34. Lindvall, O. B.; Son, N. T.; Abrikosov, I. A.; Ivády, V. Dipolar Spin Relaxation of Divacancy Qubits in Silicon Carbide. *arXiv:2102.01782*
35. Orbach, R. On the Theory of Spin-lattice Relaxation in Paramagnetic Salts. Proc. Phys. Soc. 1961, 77, 821.
36. Ivády, V. Longitudinal Spin Relaxation Model Applied to Point-defect Qubit Systems. *Phys. Rev. B* **2020**, *101*, 155203.
37. Acosta, V. M.; Bauch, E.; Ledbetter, M. P.; Waxman, A.; Bouchard, L.-S.; Budker, D. Temperature Dependence of the Nitrogen Vacancy Magnetic Resonance in Diamond. *Phys. Rev. Lett.* **2010**, *104*, 070801.

38. Chen, X. D.; Dong, C.-H.; Sun, F.-W.; Zou, C.-L.; Cui, J.-M.; Han, Z.-F.; Guo, G.-C. Temperature Dependent Energy Level Shifts of Nitrogen Vacancy Centers in Diamond. *Appl. Phys. Lett*. **2011**, *99*, 161903.
39. Doherty, M. W.; Acosta, V. M.; Jarmola, A.; Barson, M. S.; Manson, N. B.; Budker, D.; Hollenberg, L. C. L. Temperature Shifts of the Resonance of the NV^- Center in Diamond. *Phys. Rev. B* **2014**, *90*, 041201.
40. Ivády, V.; Simon, T.; Maze, J. R.; Abrikosov, I. A.; Gali, A. Pressure and Temperature Dependence of the Zero-field Splitting in the Ground State of NV Centers in Diamond: A First-Principles Study. *Phys. Rev. B* **2014**, *90*, 235205.
41. Li, Z.; Bradt, R. C. Thermal Expansion of the Cubic (3*C*) Polytype of SiC. *J. Mater. Sci*. **1986**, *21*, 4366-4368.